Energy & Environmental Science

PAPER

View Article Online
View Journal | View Issue

Cite this: *Energy Environ. Sci.*, 2016, **9**, 656

Entropic stabilization of mixed A-cation ABX_3 metal halide perovskites for high performance perovskite solar cells†

Chenyi Yi,[a] Jingshan Luo,[a] Simone Meloni,[b] Ariadni Boziki,[b] Negar Ashari-Astani,[b] Carole Grätzel,[a] Shaik M. Zakeeruddin,[a] Ursula Röthlisberger*[b] and Michael Grätzel*[a]

Received 23rd October 2015,
Accepted 2nd December 2015

DOI: 10.1039/c5ee03255e

www.rsc.org/ees

ABX_3-type organic lead halide perovskites currently attract broad attention as light harvesters for solar cells due to their high power conversion efficiency (PCE). Mixtures of formamidinium (FA) with methylammonium (MA) as A-cations show currently the best performance. Apart from offering better solar light harvesting in the near IR the addition of methylammonium stabilizes the perovskite phase of $FAPbI_3$ which in pure form at room temperature converts to the yellow photovoltaically inactive δ-phase. We observe a similar phenomenon upon adding Cs^+ cations to $FAPbI_3$. $CsPbI_3$ and $FAPbI_3$ both form the undesirable yellow phase under ambient condition while the mixture forms the desired black pervoskite. Solar cells employing the composition $Cs_{0.2}FA_{0.8}PbI_{2.84}Br_{0.16}$ yield high average PCEs of over 17% exhibiting negligible hysteresis and excellent long term stability in ambient air. We elucidate here this remarkable behavior using first principle computations. These show that the remarkable stabilization of the perovskite phase by mixing the A-cations stems from entropic gains and the small internal energy input required for the formation of their solid solution. By contrast, the energy of formation of the delta-phase containing mixed cations is too large to be compensated by this configurational entropy increase. Our calculations reveal for the first time the optoelectronic properties of such mixed A-cation perovskites and the underlying reasons for their excellent performance and high stability.

Broader context

Lead halide perovskite solar cells (PSCs) of the general formula $APbX_3$ where A stands for a monovalent cation, *i.e.* formamidinium (FA), methylammonium (MA) or Cs^+ and X for iodide or bromide are presently attracting intense research interest due to the stunning rise of their solar to electric power conversion efficiency (PCE) from 3% to 21% within a period of only a few years. Today's best PSCs use formulations composed of a mixture of formamidinium with methylammonium as A cations. Apart from offering better solar light harvesting in the near IR the addition of methylammonium leads to a striking stabilization of the perovskite phase of $FAPbI_3$ which in pure form at room temperature converts to the yellow delta phase. We observe the same phenomenon upon adding Cs^+ cations to $FAPbI_3$. $CsPbI_3$ and $FAPbI_3$ both form the undesirable yellow phase under ambient condition while the mixture forms the desired black pervoskite. We elucidate here, for the first time, this remarkable behavior using first principle computations. Our theoretical analysis shows that the remarkable stabilization of the perovskite phase by mixing the A-cations stems from entropic gains and the small internal energy input required for the formation of their solid solution. In contrast, the energy of formation of the delta-phase (yellow) containing a mixture of the same cations is too large to be compensated by the configurational entropy increase. Our band structure calculations explain the effect of cation and anion mixing on the opto-electronic properties of the materials which should foster their future development as key energy conversion materials.

Introduction

Organic inorganic hybrid metal halide perovskites have been under intense investigation following their initial use as light harvesting pigments in dye-sensitized solar cells.[1–4] When using optimized fabrication procedures judiciously chosen perovskite formulations exhibit broad absorption spectra with sharp edges in the near infrared making them excellent light

[a] *Laboratory of Photonics and Interfaces, Institute of Chemical Sciences and Engineering, School of Basic Sciences, Ecole Polytechnique Federale de Lausanne, CH-1015 Lausanne, Switzerland. E-mail: michael.graetzel@epfl.ch*
[b] *Laboratory of Computational Chemistry and Biochemistry, Institute of Chemical Sciences and Engineering, Ecole Polytechnique Federale de Lausanne, CH-1015 Lausanne, Switzerland*

† Electronic supplementary information (ESI) available. See DOI: 10.1039/c5ee03255e

harvesters that demonstrate properties as either n- or p-type semiconductors with close to optimal band gaps for solar energy conversion. These favorable characteristics coupled with long carrier diffusion lengths and the feasibility of their fabrication by solution processing, leading to low production costs, make them excellent candidates as opto-electronic materials.[5–17] Methylammonium lead iodide ($MAPbI_3$) has been the most widely studied ABX_3 (where A is the organic (or inorganic) cation, B is the divalent metal cation and X the halide anion) structured perovskite material up until now. However, it decomposes rapidly at higher temperatures exhibiting discoloration after heating at 150 °C for 30 minutes in air.[18] Formamidinium lead iodide ($FAPbI_3$) has emerged as a promising candidate for use in perovskite solar cells (PSCs), primarily due to its absorption spectrum that extends further into the red than that of $MAPbI_3$, potentially leading to higher current densities.[18–20] Moreover, $FAPbI_3$ is more resistant to heat stress than $MAPbI_3$ although both show degradation in ambient air at relative humidities approaching 100%.[18] However, the black perovskite phase of pure $FAPbI_3$, is thermodynamically stable only above 160 °C,[12] forming a yellow δ phase below the phase transition temperature. To stabilize the perovskite phase of $FAPbI_3$ at room temperature, $MAPbI_3$ has been added to produce mixed cation PSCs.[19] These mixed $(MAPbX_3)_x(FAPbI_3)_{1-x}$ perovskites were utilized in the fabrication of solar cells and exhibit the highest power conversion efficiencies to date with certified values exceeding 20%.[11,12,19] However, the mixed $(MAPbX_3)_x(FAPbI_3)_{1-x}$ perovskite is also prone to decomposition under heat stress, due to the presence of $MAPbX_3$. Hence it is of great importance to develop a perovskite structure that is stable in both low and high temperature ranges.

Purely inorganic perovskites of the general formula, $CsPbX_3$, such as $CsPbI_3$ and $CsPbBr_3$, are drawing attention for use as luminescent materials and in high-energy radiation detectors.[21–26] Perovskite solar cells utilizing $CsPbBr_3$ have exhibited excellent thermal stability with high photovoltages.[27] However, the photocurrent is low due to the wide band gap (2.36 eV) of the light absorber. The perovskite phase of $CsPbI_3$ has a narrower band gap (1.73 eV) than $CsPbBr_3$; however, the perovskite phase of $CsPbI_3$ is only stable at high temperature, converting to the yellow (δ) phase under room temperature conditions.[28] In fact, the first-order reversible phase transition of $CsPbI_3$ from a yellow orthorhombic phase to a dark cubic perovskite phase takes place at 308 °C[24,29] preventing its use in practical applications such as solar cells. Cesium doped $MAPbI_3$ perovskites, were likewise employed in solar cells, demonstrating higher voltages than pure $MAPbI_3$. However, the best reported solar to electric power conversion efficiency (PCE) of the cesium doped $MAPbI_3$ perovskite is 7.68%.[30]

Here we present a $MAPbX_3$-free mixed cation perovskite, $Cs_xFA_{(1-x)}PbX_3$, as an attractive material for perovskite solar cells exhibiting both high efficiencies and good thermal stability. Although both $FAPbI_3$ and $CsPbI_3$ 3D perovskite phases are unstable at room temperature, room temperature stable $Cs_{0.2}FA_{0.8}PbI_3$ perovskite is formed by adding 20% $CsPbI_3$ into $FAPbI_3$. The film darkens immediately upon the adjunction of the anti-solvent chlorobenzene at room temperature. Moreover, the new perovskite is also stable at higher temperatures. Here we elucidate, for the first time, this remarkable behavior using first principle computations. Our theoretical analysis includes band structure calculations that explain the effect of cation and anion mixing on the opto-electronic properties of the materials. We fabricate mixed cation PSCs with a high PCE, the average being above 15%, exceeding the efficiency reached with pure $FAPbI_3$ perovskite. The mixed cation perovskite shows good stability with no discernible decrease in efficiency of unsealed solar cells following a time lapse of 1000 h under ambient conditions in the dark. We note that our experimental results agree with those of a very recent study that appeared during the final preparation of our manuscript that investigates similar mixed cation PSCs.[31] We find that the PCE can be further improved up to 18% by replacing a small fraction of the iodide in the mixed cation perovskite with bromide anions.

Results and discussion

We produced the perovskite film by spin coating a $Cs_xFA_{1-x}PbX_3$ solution on a mesoporous TiO_2 film. The precursor solution is made by dissolving CsI, formamidinium iodide and formamidinium bromide (for mixed halide devices) with PbI_2 in a mixture of DMF and DMSO. At the last stage of the spin coating, the film is treated with chlorobenzene, as antisolvent, to improve the perovskite crystallization. Following spin coating, the film is annealed at 100 °C for 30 minutes. Perovskite films produced in this manner turn dark immediately after spin coating and subsequent heating, suggesting the formation of the black perovskite (*versus* δ) phase of the $Cs_{0.2}FA_{0.8}PbI_3$. On the contrary, a spin-coated film of $FAPbI_3$ remains yellow in color even after heating at 100 °C for more than 30 minutes, darkening only at temperatures of 150 °C and above.

The effects of the added Cs and Br on the absorption properties of the $FAPbI_3$ perovskite have been examined by using UV-vis absorption. The absorption spectra Fig. 1a indicate a slight blue shift of 5 nm upon increasing the ratio of Cs in $Cs_xFA_{(1-x)}PbI_3$ from 0 to 0.4, in good agreement with theoretical calculations, suggesting only a minor effect of Cs on the band gap of the perovskite. On the contrary, a significant blue shift from 785 nm to 735 nm is observed when increasing the content of Br added into the perovskite structure, from $Cs_{0.2}FA_{0.8}PbI_3$ to $Cs_{0.2}FA_{0.8}PbI_{2.6}Br_{0.4}$, as shown in Fig. 1b. This observation indicates that the band gap augments with increasing concentration of Br in the inorganic organic hybrid lead iodide/bromide perovskites, confirming our theoretical calculations. Although the blue spectral shift decreases the maximum theoretical photocurrent density of the device, it is possible to obtain higher voltages when using the larger band gap absorption materials. Photoluminescence spectra, Fig. 1c, show a similar trend of blue shift of emission maximum from 806 nm to 772 nm by increasing the Br concentration from $Cs_{0.2}FA_{0.8}PbI_3$ to $Cs_{0.2}FA_{0.8}PbI_{2.6}Br_{0.4}$. By contrast, increasing the Cs concentration from 0 to 0.4 for $Cs_xFA_{(1-x)}PbI_3$ shifts the emission spectra towards the blue by only a few nm. Fig. 1d shows the intersection point of absorption and emission spectra of $Cs_{0.2}FA_{0.8}PbI_3$ and $Cs_{0.2}FA_{0.8}PbI_{2.84}Br_{0.16}$

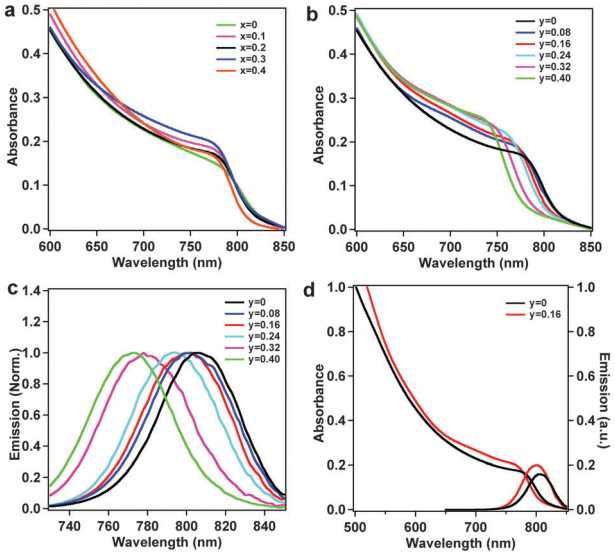

Fig. 1 Photophysical properties of $Cs_xFA_{(1-x)}PbI_3$ and $Cs_{0.2}FA_{0.8}PbI_{(3-y)}Br_y$. (a) UV-vis spectra of mixed A cation perovskites of different mixing ratios $Cs_xFA_{(1-x)}PbI_3$. (b) Effect of substitution of iodide by bromide on the UV-vis spectra of $Cs_{0.2}FA_{0.8}PbI_{(3-y)}Br_y$. (c) Normalized photoluminescence spectra of $Cs_{0.2}FA_{0.8}PbI_{(3-y)}Br_y$. (d) Absorption and emission spectra of $Cs_{0.2}FA_{0.8}PbI_3$ (black) and $Cs_{0.2}FA_{0.8}PbI_{2.84}Br_{0.16}$ (red).

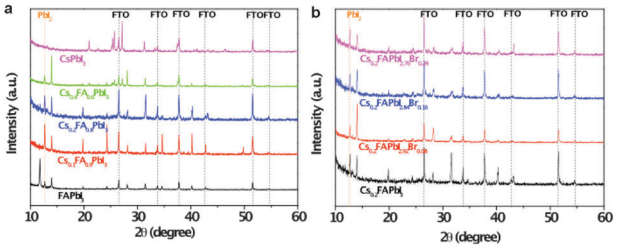

Fig. 2 (a) XRD spectra of $FAPbI_3$, $CsPbI_3$ and the $Cs_xFA_{(1-x)}PbI_3$. (b) Effect of iodide substitution by bromide on the XRD spectra of $Cs_{0.2}FA_{0.8}PbI_{(3-y)}Br_y$.

are at 792 nm and 782 nm respectively, corresponding to band gaps of 1.56 eV and 1.58 eV.

Differential scanning calorimetry (DSC) was employed to investigate the thermal behavior of the mixed perovskites. Fig. S1 (ESI†) shows the DSC scans of the perovskites from 20 °C to 250 °C under nitrogen gas atmosphere. Neither of the mixed perovskites, $Cs_{0.2}FA_{0.8}PbI_3$ and $Cs_{0.2}FA_{0.8}PbI_{2.84}Br_{0.16}$, shows any peaks, indicating that the perovskite phase of this type of mixed perovskites is stable over the investigated temperature range. On the contrary, the pure $FAPbI_3$ exhibits a peak at 156 °C, indicating a phase transition of $FAPbI_3$ from the yellow δ phase to the perovskite structure at this temperature. This finding is consistent with the color change of the $FAPbI_3$ film from yellow to black at around 150 °C. The thermal stability of the mixed perovskites was investigated by heating the film at 150 °C in ambient air. Whereas $Cs_{0.2}FA_{0.8}PbI_3$ and $Cs_{0.2}FA_{0.8}PbI_{2.84}Br_{0.16}$ are stable, showing no discoloration, the $MAPbI_3$ color changes from dark-brown to yellow after 60 minutes. The $(MAPbBr_3)_{0.15}(FAPbI_3)_{0.85}$ perovskite likewise discolors following 60 minutes heating.

Fig. 2a shows the XRD spectra of the $Cs_xFA_{1-x}PbI_3$ and that of $FAPbI_3$ annealed at 150 °C. Annealing produces the trigonal perovskite phase of $FAPbI_3$. However, the intense peak at 11.7 degrees indicates that the hexagonal non-perovskite δ phase still exists after the heat treatment in agreement with previous work.[12] The peak at 12.7 degrees corresponds to the hexagonal phase of PbI_2. Remarkably, when 10% Cs was added to the $FAPbI_3$, the formation temperature of the perovskite phase decreased sharply allowing formation of the trigonal perovskite phase to occur already at room temperature. This suggests that the introduction of Cs thermodynamically favors the formation of the perovskite phase, bringing the system into a new equilibrium state. This supposition will be substantiated below by theoretical analysis. Increasing the Cs^+ content beyond 10% does not seem to impact the formation of the perovskite phase. However, when its concentration reaches 40% or above, the peaks at 25.4 and 28.1 degrees become more visible and split into two, due to the larger distortion of the perovskite lattice, in good agreement with the theoretical calculations (Fig. S11, ESI†). We substituted a small fraction of iodide by bromide in the perovskite lattice to further boost the efficiency.[12] No changes in the phase of film occurred upon increasing the Br concentration. Even for the formulation with the highest concentration of Br of 13 mol% ($Cs_{0.2}FA_{0.8}PbI_{2.6}Br_{0.4}$) employed here, the film still remained in the trigonal perovskite phase, in agreement with previous studies showing that iodine rich perovskites remain in the trigonal phase, while Br rich ones form the cubic phase.[18,32]

The Pb 4f core level signals for different samples are shown in Fig. S2 (ESI†). The $Cs_{0.2}FA_{0.8}PbI_3$ sample exhibits two dominant peaks located at 137.1 eV and 141.9 eV, corresponding to the Pb $4f_{7/2}$ and Pb $4f_{5/2}$ level, respectively, indicating a spin–orbit splitting of 4.8 eV. The small satellites at low binding energy are, according to previous reports,[33] due to metallic lead. After Br doping, the Pb^{2+} lines show a 0.3 eV binding energy shift to a higher energy level, which could be attributed to the fact that Pb 6s orbitals have a larger overlap with the p-orbitals of iodide than bromide. All samples show strong signals from I 3d and Cs 3d core levels, and their peaks don't show any apparent shift when Br is incorporated into the structure. For the I 3d core level, following Br doping, the intensity of peaks decreased, concomitant with the decrease of I concentration in the sample. Pure $Cs_{0.2}FA_{0.8}PbI_3$ has no signal in the region of the Br core level. After incorporation of Br, the peaks assigned to Br 3d become visible, and the intensity increases as expected as a function of the Br concentration.

The morphology of the film has been investigated by scanning electron microscopy (SEM). Fig. 3a shows the cross-sectional SEM image of the perovskite solar cell device. From bottom to top, the device consists of successive layers of FTO, compact TiO_2, mesoporous TiO_2/perovskite composite, perovskite capping layer, spiro-OMeTAD hole transporting material (HTM) and gold (Au) as counter electrode. The perovskite capping layer lies in a homogenous layer on top of the mesoporous TiO_2/perovskite composite, separating the HTM from possible contact with TiO_2. This conformal capping layer helps prevent charge recombination between the HTM and the electron transporter, TiO_2. Fig. 3b shows the top view SEM image of the $Cs_{0.2}FA_{0.8}PbI_3$ perovskite film.

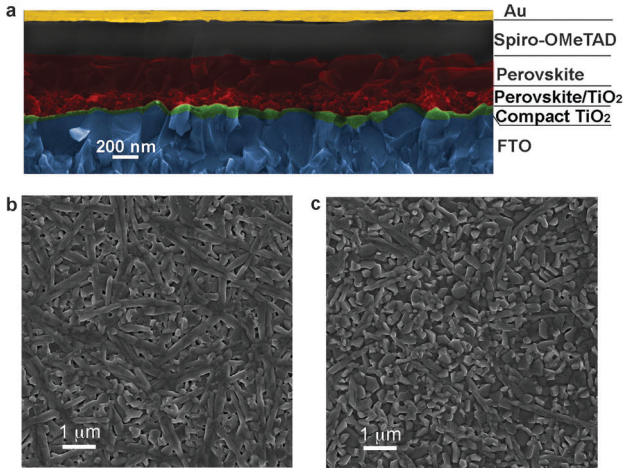

Fig. 3 (a) Cross-sectional SEM image of a complete photovoltaic device. (b) Top-view SEM image of the $Cs_{0.2}FA_{0.8}PbI_3$ perovskite. (c) Top-view SEM image of the $Cs_{0.2}FA_{0.8}PbI_{2.84}Br_{0.16}$ perovskite.

It indicates a branchlike structural morphology of the perovskite crystal grains with good surface coverage. As observed in the top view SEM image of $Cs_{0.2}FA_{0.8}PbI_{2.84}Br_{0.16}$, Fig. 3c, its morphology is similar to that of $Cs_{0.2}FA_{0.8}PbI_3$. Both the pure iodide and bromide containing perovskites' uniform and compact layer formation on the mesoporous TiO_2 are consistent with the cross-sectional SEM results.

A high-resolution transmission electron microscopy (TEM) image, Fig. S3 (ESI†), shows periodically aligned parallel lines resulting from the crystalline planes, indicating the high level of crystallinity of the perovskite granular structure. A high-angle annular dark-field scanning transmission electron microscopy (HAADF-STEM) image, Fig. 4, illustrates the morphology of the perovskite grains, which was analyzed by scanning transmission electron microscopy energy dispersive spectroscopy (STEM-EDS). The STEM-EDS mapping of Cs, Pb, I, Br exhibits a similar pattern compared to the image of HAADF-STEM. These findings signify that the elements Cs, Pb, I, Br are homogeneously distributed within the perovskite crystals, suggesting that the Cs and Br are uniformly incorporated into the $FAPbI_3$ in the perovskite grain rather than existing in separate chemical phases.

We find that the remarkable stabilization of the perovskite over the non-perovskite δ phase upon Cs/FA mixing can be rationalized with simple structural and thermodynamic arguments. The δ phases of $FAPbI_3$ and $CsPbI_3$ differ significantly in their atomistic structure. In the case of the $FAPbI_3$, the δ-phase consists of 1D pillars made of face sharing PbI_6 octahedra (Fig. 5a). These pillars, aligned along the crystallographic c direction, are separated by domains containing only FA. The δ-$CsPbI_3$ crystal is also made of 1D PbI_3 pillars surrounded by the cation, Cs^+ in this case, but these pillars consist of stacked and shifted edge sharing PbI_6 octahedra (Fig. 5b). Another significant difference is the volume per stoichiometric unit of the two systems: (Vδ-$FAPbI_3$ ∼ 256 Å^3 *vs.* Vδ-$CsPbI_3$ ∼ 222 Å^3 [32]). On the contrary, the α and β perovskite $FAPbI_3$ phases (Fig. 5c and d) are very similar to the perovskite phase of $CsPbI_3$ (Fig. 5e), and the volume per stoichiometric unit of the three crystals is also very close (Vα-$FAPbI_3$ ∼ 256 Å^3 and Vβ-$FAPbI_3$ ∼ 249 Å^3 [28,32] *vs.* Vα-$CsPbI_3$ ∼ 250 Å^3 [28,32]). This suggests that cation mixing in

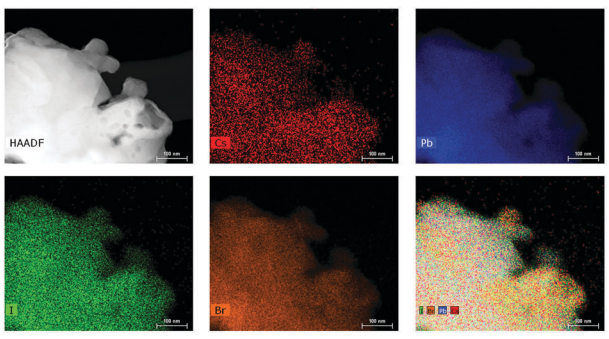

Fig. 4 HAADF and TEM-EDS image of $Cs_{0.2}FA_{0.8}PbI_{2.84}Br_{0.16}$.

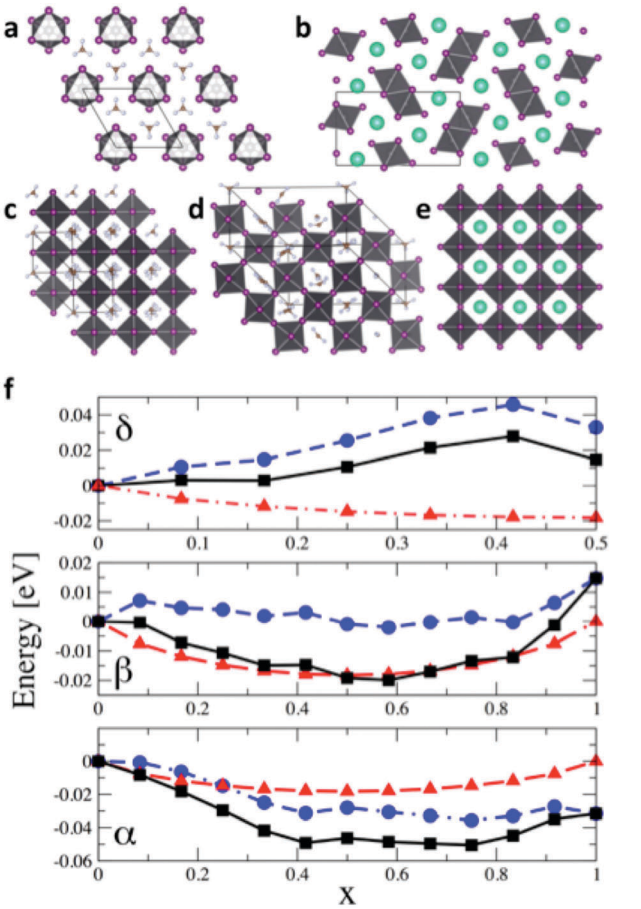

Fig. 5 Various phases of $FAPbI_3$ and $CsPbI_3$ and variation of internal energy of mixed $Cs_xFA_{1-x}PbI_3$ in different phases. (a and b) Represent the δ phase in the FA and Cs perovskites, respectively; (c and d) show the α and β $FAPbI_3$, respectively. (e) Shows the cubic phase of the $CsPbI_3$ structure. Comparison between the structures reported in panels (a) and (b), and panels (b), (c) and (e) highlights the significant difference in the δ structure of FA and Cs lead iodide, as opposed to the strong similarities in the corresponding perovskite phases. (f) Variation of internal energy, ΔE (dashed blue line), mixing entropy contribution, $-T\Delta S$ (dot-red dashed line), and free energy, $\Delta F = \Delta E - T\Delta S$ (black continuous line) as a function of Cs content.

the δ phase is energetically highly unfavorable, while it is more favorable for the perovskite α and β phases. According to this hypothesis, in the δ phase the unfavorable energetic contribution due to mixing is too large to be compensated by the mixing entropy. On the contrary, in the α and β perovskite phases the sum of the energy and mixing entropy contribution leads to a reduction of the free energy, resulting in a stabilization of the mixed 3D perovskite over the δ phase. Since Cs and FA are mixed in solution, thanks to the stability enhancement the perovskite phase forms directly, before the separated δ-phases can prevent mixing. This hypothesis is confirmed by the results shown in Fig. 5f where the energy and mixing entropy contributions to the free energy, together with their sum, are plotted as a function of the Cs content, in the compounds comprising $Cs_xFA_{1-x}PbI_3$ in their α, β, and δ phases.

Analysis of the energetics in the δ phase shows that replacement of the organic cation FA^+ by the inorganic cation Cs^+ leads to a significant destabilization (energy increase) with respect to the two pure FA and/or $CsPbI_3$ δ phases, ΔEδ-$Cs_xFA_{1-x}PbI3 = E$δ-$Cs_xFA_{1-x}PbI_3 - (xE$δ-$Cs_xPbI + (1 - x)E$δ-$FA_{1-x}PbI)$. The mixing entropy contribution to the free energy, $T\Delta S$δ-$Cs_xFA_{1-x}PbI_3 = k_BT[x\log x + (1 - x)\log(1 - x)]$, does not compensate this energetic penalty and, as hypothesized above, cation mixing cannot take place in the δ phase. On the contrary, for the perovskite phases, either the α and β types, the sum of the energetic and mixing entropy contributions to the free energy is favorable, resulting in a stabilization of the mixed phases (see ESI† for more details). This stabilization is of the order of 0.05 eV ($\sim 2k_BT$ at room temperature) and 0.02 eV ($\sim 0.8\ k_BT$) per stoichiometric unit for the α and β phase, respectively. Within this simple model, the δ → α or β transition temperature is reduced by ~200–300 K when going from the pure $FAPbI_3$ to the mixed $Cs_xFA_{1-x}PbI_3$ system, which explains why the perovskite phase is stable at room temperature for the mixed compound. The increase of compound stability upon mixing may also account for the observed resistance towards decomposition at higher temperatures of mixed cation perovskites.

Fig. 5f shows that the maximum stabilization is achieved at 40–60% Cs content. However, this might not be the best composition to maximize the efficiency of the solar cell. Thus, in the following we investigate how A-cation mixing affects the electronic properties of perovskites. Cation mixing alters the electronic structure of the perovskite in two ways. First, it leads to a slight widening of the band gap (Fig. S4, ESI†), which is blue-shifted by ~15 nm in the case of β-$Cs_{0.25}(FA)_{0.75}PbI_3$, in good agreement with the experimental results. This shift arises from the distortion of the PbI_3 lattice upon mixing, with the average Pb–I–Pb angle passing from 167° in the pure β FA-perovskite to 164.5° at ~25% Cs mixing (more details are given in the ESI†). The distortion of the lattice reduces the p-I/s-Pb antibonding overlap of the valence band maximum (VBM, see Fig. S5a/b, ESI†), resulting in a reduction of its energy and an increase of the bandgap. A second effect of cation mixing is an increase of the density of states (DOS) in the region up to 0.5 eV below the VBM, which is consistent with the observed increase of the IPCE. Summarizing, concerning the electronic and optical properties, the optimal Cs content is the result of a trade-off between the opposing effects of the Cs concentration on the band structure, *i.e.*, the widening of the band gap and the increase of the DOS in the sub-VBM region.

Replacement of iodide with a limited amount of bromide in mixed Cs/FA perovskites, is thermodynamically favored for both the α and β phases (Fig. S6, ESI†). The band structure of β-$Cs_{0.25}FA_{0.75}PbI_{3-y}Br_y$ is shown in Fig. S7 (ESI†). The main effect of substituting iodide by bromide on the pervoskite lattice is a widening of the bandgap consistent with the observed blue shift of the absorption edge (*vide infra*). This increase of the bandgap is due to a decrease of the antibonding overlap between the X-*n*p (X = Br or I) and Pb-6s orbitals with respect to the pure iodide perovskite. There are two reasons for this effect. On the one hand, the different size of I and Br ions further distorts the $PbI_{3-y}Br_y$ framework, resulting in a reduction of the Pb-6s/I-5p overlap (Fig. S8, ESI†). Moreover, the more compact Br-4p orbital has a limited antibonding overlap with the Pb-6s in the inorganic framework that, at the compositions investigated, has a size that is still close to that of the corresponding iodide perovskite.

The photovoltaic properties of the perovskites were ascertained by measuring the current–voltage (*J–V*) curves and by evaluating the devices' corresponding incident-photon-to-current conversion efficiency (IPCE) spectra. The representative *J–V* curves and their corresponding PV parameters are illustrated in Fig. 6 and tabulated in Table 1, respectively. The device fabricated by pure $FAPbI_3$ perovskite films gives a power conversion efficiency (PCE) of 10.4% with open-circuit voltage (V_{oc}) of 809 mV, short circuit current density (J_{sc}) of 21.4 mA cm^{-2} and a fill factor of 59.2%. Following incorporation of Cs, the mixed cation perovskite $Cs_{0.2}FA_{0.8}PbI_3$ device yields an enhanced PCE (compared to pure $FAPbI_3$) of 15.69%, with PV parameters of V_{oc} = 1017 mV, J_{sc} = 21.5 mA cm^{-2} and fill factor = 70.1%. Substituting 5% of the iodide in the mixed cation perovskite by bromide yielding the $Cs_{0.2}(FA)_{0.8}PbI_{2.84}Br_{0.16}$, improves the PCE further to a value of 17.35%, with V_{oc} = 1073 mV, J_{sc} = 21.9 mA cm^{-2} and a fill factor of 74.2%. The champion cell shows an overall PCE of 18.02%, with a V_{oc} of 1072 mV, a J_{sc} of 23.3 mA cm^{-2} and a fill factor of 72.3%. Moreover, preliminary stability tests show that the device based on $Cs_{0.2}FA_{0.8}PbI_3$ is much more stable than $FAPbI_3$ under ambient conditions when kept unsealed in the dark. The device based on $Cs_{0.2}FA_{0.8}PbI_3$ (Fig. S10, ESI†) shows no performance decrease within 1000 h. The bromide doped perovskite's performance Fig. 6c matches that of the pure iodide mixed cation perovskite. On the contrary, perovskite solar cell based on pure $FAPbI_3$ degrades within 48 h under the same conditions. As shown in Fig. 6b, the onset of the IPCE spectra for the $Cs_{0.2}FA_{0.8}PbI_3$ device is at 860 nm and that for the $Cs_{0.2}FA_{0.8}PbI_{2.84}Br_{0.16}$ device is at 830 nm, agreeing well with the UV-vis spectra. On the other hand a somewhat higher overall IPCE value is observed for the $Cs_{0.2}FA_{0.8}PbI_{2.84}Br_{0.16}$ device compared to the pure iodide device, probably due to its higher absorbance and longer carrier diffusion length.[10] The integrated current densities calculated from the IPCE spectra agree well with the corresponding measured photocurrent densities,

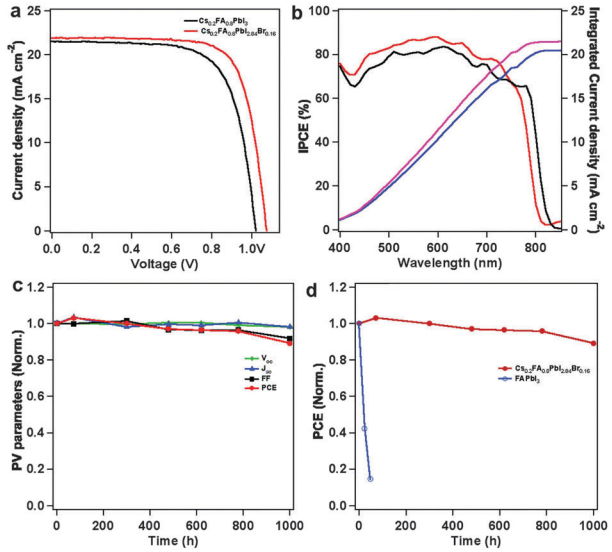

Fig. 6 Photovoltaic properties of $Cs_{0.2}FA_{0.8}PbI_3$ and $Cs_{0.2}FA_{0.8}PbI_{2.84}Br_{0.16}$ perovskite solar cells. (a) *J–V* curves of the $Cs_{0.2}FA_{0.8}PbI_3$ and $Cs_{0.2}FA_{0.8}PbI_{2.84}Br_{0.16}$ perovskite solar cells. (b) IPCE spectra of the $Cs_{0.2}FA_{0.8}PbI_3$ (black) and $Cs_{0.2}FA_{0.8}PbI_{2.84}Br_{0.16}$ (red) perovskite solar cells and their integrated currents $Cs_{0.2}FA_{0.8}PbI_3$ (blue) and $Cs_{0.2}FA_{0.8}PbI_{2.84}Br_{0.16}$ (purple). (c) Evolution of the photovoltaic parameters with time for the $Cs_{0.2}FA_{0.8}PbI_{2.84}Br_{0.16}$ perovskite solar cells. The unsealed solar cells were kept under ambient conditions in the dark and the performances were re-evaluated at periodic intervals. (d) Comparison of the stability of $Cs_{0.2}FA_{0.8}PbI_{2.84}Br_{0.16}$ and $FAPbI_3$ perovskite solar cells, conditions as in (c).

Table 1 Photovoltaic parameters of the pure FA and the doped Cs and Br PSCs

Composition	J_{sc} (mA cm^{-2})	V_{oc} (mV)	FF (%)	PCE (%)
$FAPbI_3$	21.4	809	59.2	10.4
$Cs_{0.2}FA_{0.8}PbI_3$	21.5	1017	70.1	15.69
$Cs_{0.2}FA_{0.8}PbI_{2.84}Br_{0.16}$	21.9	1073	74.2	17.35

indicating that the emission of our solar simulator matches well the spectrum of standard air mass 1.5 solar light.

Conclusions

We have demonstrated that a mixed A cation inorganic–organic perovskite prepared by incorporating Cs into $FAPbI_3$ can be used to produce high performance solar cells. These perovskite films are homogeneous and can be conformally coated onto the TiO_2 photoanode, showing no separation into different chemical phases. They can be produced at temperatures lower than the 150 °C required for the pure $FAPbI_3$ films, remaining stable with no (reversible) phase transitions to the inactive, yellow colored, δ phase, over a large temperature range down to room temperature. This stabilization can be rationalized in terms of the miscibility of $CsPbI_3$ and $FAPbI_3$ in the perovskite phase, while the same compounds are not miscible in the δ phase due to the fact that $CsPbI_3$ and $FAPbI_3$ are very similar in the atomistic structure and volume in the former but not in the latter. This results in large energy penalty for mixing in the δ phases, while the mixing of the perovskite phases is energetically favorable. The high performance of the mixed $Cs_xFA_{(1-x)}PbI_3$ perovskite exemplifies the great potential of this newly developed material not only in the production of high efficiency solar cells, but also as materials for optoelectronic devices such as photoconductors and OLEDs.

Acknowledgements

The authors would like to thank Dr Pierre Mettraux in Molecular and Hybrid Materials Characterization Center, EPFL for carrying out XPS measurements. M. G. acknowledges financial support from SNF-NanoTera (SYNERGY), CCEM-CH in the 9th call proposal 906: CONNECT PV and the Swiss National Science Foundation (SNF)-NRP70 "Energy Turnaround" (PV2050, 407040-153990/1, 407040-153976/1, 407040-153916/1 and 407040-153952/1). J. L. would like to thank EPFL Fellowship co-funded by Marie Curie from the European Union's Seventh Framework Programme for research, technological development and demonstration under grant agreement no. 291771. S. M., A. B., N. A. A., and U. R. acknowledge PRACE for awarding us access to resource Supermuc based in Germany at LRZ. This work was supported by a grant from the Swiss National Supercomputing Centre (CSCS) under project ID s426 and a grant from the King Abdulaziz City of Science and Technology (KACST), Riyadh, Saudi Arabia.

Notes and references

1 A. Kojima, K. Teshima, Y. Shirai and T. Miyasaka, *J. Am. Chem. Soc.*, 2009, **131**, 6050–6051.
2 J. H. Im, C. R. Lee, J. W. Lee, S. W. Park and N. G. Park, *Nanoscale*, 2011, **3**, 4088–4093.
3 I. Chung, B. Lee, J. Q. He, R. P. H. Chang and M. G. Kanatzidis, *Nature*, 2012, **485**, 486–489.
4 H. S. Kim, C. R. Lee, J. H. Im, K. B. Lee, T. Moehl, A. Marchioro, S. J. Moon, R. Humphry-Baker, J. H. Yum, J. E. Moser, M. Gratzel and N. G. Park, *Sci. Rep.*, 2012, **2**, 591.
5 M. M. Lee, J. Teuscher, T. Miyasaka, T. N. Murakami and H. J. Snaith, *Science*, 2012, **338**, 643–647.
6 G. C. Xing, N. Mathews, S. Y. Sun, S. S. Lim, Y. M. Lam, M. Gratzel, S. Mhaisalkar and T. C. Sum, *Science*, 2013, **342**, 344–347.
7 A. Y. Mei, X. Li, L. F. Liu, Z. L. Ku, T. F. Liu, Y. G. Rong, M. Xu, M. Hu, J. Z. Chen, Y. Yang, M. Gratzel and H. W. Han, *Science*, 2014, **345**, 295–298.
8 H. P. Zhou, Q. Chen, G. Li, S. Luo, T. B. Song, H. S. Duan, Z. R. Hong, J. B. You, Y. S. Liu and Y. Yang, *Science*, 2014, **345**, 542–546.
9 Q. F. Dong, Y. J. Fang, Y. C. Shao, P. Mulligan, J. Qiu, L. Cao and J. S. Huang, *Science*, 2015, **347**, 967–970.
10 D. Shi, V. Adinolfi, R. Comin, M. J. Yuan, E. Alarousu, A. Buin, Y. Chen, S. Hoogland, A. Rothenberger, K. Katsiev, Y. Losovyj, X. Zhang, P. A. Dowben, O. F. Mohammed, E. H. Sargent and O. M. Bakr, *Science*, 2015, **347**, 519–522.
11 W. S. Yang, J. H. Noh, N. J. Jeon, Y. C. Kim, S. Ryu, J. Seo and S. I. Seok, *Science*, 2015, **348**, 1234–1237.

12 N. J. Jeon, J. H. Noh, W. S. Yang, Y. C. Kim, S. Ryu, J. Seo and S. I. Seok, *Nature*, 2015, **517**, 476–480.
13 J. Burschka, N. Pellet, S. J. Moon, R. Humphry-Baker, P. Gao, M. K. Nazeeruddin and M. Gratzel, *Nature*, 2013, **499**, 316–319.
14 M. Z. Liu, M. B. Johnston and H. J. Snaith, *Nature*, 2013, **501**, 395–398.
15 N. J. Jeon, J. H. Noh, Y. C. Kim, W. S. Yang, S. Ryu and S. Il Seol, *Nat. Mater.*, 2014, **13**, 897–903.
16 Z. G. Xiao, Q. F. Dong, C. Bi, Y. C. Shao, Y. B. Yuan and J. S. Huang, *Adv. Mater.*, 2014, **26**, 6503–6509.
17 T. Y. Zhang, M. J. Yang, Y. X. Zhao and K. Zhu, *Nano Lett.*, 2015, **15**, 3959–3963.
18 G. E. Eperon, S. D. Stranks, C. Menelaou, M. B. Johnston, L. M. Herz and H. J. Snaith, *Energy Environ. Sci.*, 2014, **7**, 982–988.
19 N. Pellet, P. Gao, G. Gregori, T. Y. Yang, M. K. Nazeeruddin, J. Maier and M. Gratzel, *Angew. Chem., Int. Ed.*, 2014, **53**, 3151–3157.
20 J. W. Lee, D. J. Seol, A. N. Cho and N. G. Park, *Adv. Mater.*, 2014, **26**, 4991–4998.
21 H. Ito, H. Onuki and R. Onaka, *J. Phys. Soc. Jpn.*, 1978, **45**, 2043–2044.
22 C. C. Stoumpos, C. D. Malliakas, J. A. Peters, Z. F. Liu, M. Sebastian, J. Im, T. C. Chasapis, A. C. Wibowo, D. Y. Chung, A. J. Freeman, B. W. Wessels and M. G. Kanatzidis, *Cryst. Growth Des.*, 2013, **13**, 2722–2727.
23 L. Protesescu, S. Yakunin, M. I. Bodnarchuk, F. Krieg, R. Caputo, C. H. Hendon, R. X. Yang, A. Walsh and M. V. Kovalenko, *Nano Lett.*, 2015, **15**, 3692–3696.
24 D. Zhang, S. W. Eaton, Y. Yu, L. Dou and P. Yang, *J. Am. Chem. Soc.*, 2015, **137**, 9230–9233.
25 Q. A. Akkerman, V. D'Innocenzo, S. Accornero, A. Scarpellini, A. Petrozza, M. Prato and L. Manna, *J. Am. Chem. Soc.*, 2015, **137**, 10276–10281.
26 G. Nedelcu, L. Protesescu, S. Yakunin, M. I. Bodnarchuk, M. J. Grotevent and M. V. Kovalenko, *Nano Lett.*, 2015, **15**, 3692–3696.
27 M. Kulbak, D. Cahen and G. Hodes, *J. Phys. Chem. Lett.*, 2015, **6**, 2452–2456.
28 D. M. Trots and S. V. Myagkota, *J. Phys. Chem. Solids*, 2008, **69**, 2520–2526.
29 C. K. Moller, *Nature*, 1958, **182**, 1436.
30 H. Choi, J. Jeong, H. B. Kim, S. Kim, B. Walker, G. H. Kim and J. Y. Kim, *Nano Energy*, 2014, **7**, 80–85.
31 J.-W. Lee, D.-H. Kim, H.-S. Kim, S.-W. Seo, S. M. Cho and N.-G. Park, *Adv. Energy Mater.*, 2015, DOI: 10.1002/aenm.201501310.
32 C. C. Stoumpos, C. D. Malliakas and M. G. Kanatzidis, *Inorg. Chem.*, 2013, **52**, 9019–9038.
33 R. Lindblad, D. Q. Bi, B. W. Park, J. Oscarsson, M. Gorgoi, H. Siegbahn, M. Odelius, E. M. J. Johansson and H. Rensmo, *J. Phys. Chem. Lett.*, 2014, **5**, 648–653.

